SUBMITTED TO APJ
Preprint typeset using LaTeX style emulateapj v. 11/12/01

SOLAR-LIKE OSCILLATIONS IN α CENTAURI B

HANS KJELDSEN,[1] TIMOTHY R. BEDDING,[2] R. PAUL BUTLER,[3] JØRGEN CHRISTENSEN-DALSGAARD,[1]
LASZLO L. KISS,[2] CHRIS MCCARTHY,[3] GEOFFREY W. MARCY,[4] CHRISTOPHER G. TINNEY[5] AND JASON T. WRIGHT[4]
Submitted to ApJ

ABSTRACT

We have made velocity observations of the star α Cen B from two sites, allowing us to identify 37 oscillation modes with l = 0–3. Fitting to these modes gives the large and small frequency separations as a function of frequency. The mode lifetime, as measured from the scatter of the oscillation frequencies about a smooth trend, is similar to that in the Sun. Limited observations of the star δ Pav show oscillations centred at 2.3 mHz with peak amplitudes close to solar. We introduce a new method of measuring oscillation amplitudes from heavily-smoothed power density spectra, from which we estimated amplitudes for α Cen A and B, β Hyi, δ Pav and the Sun. We point out that the oscillation amplitudes may depend on which spectral lines are used for the velocity measurements.

Subject headings: stars: individual (α Cen A, α Cen B, β Hyi, δ Pav) — stars: oscillations — Sun: helioseismology

1. INTRODUCTION

The α Cen A & B system is an excellent target for asteroseismology. Velocity oscillations in the A component were measured by Bouchy & Carrier (2001, 2002) and subsequently by Butler et al. (2004, see also Bedding et al. 2004). The first detection of oscillations in α Cen B (HR 5460) was made by Carrier & Bourban (2003), based on velocity measurements with the CORALIE spectrograph in Chile spanning 13 nights. They observed excess power centred at 4 mHz and used the autocorrelation of the power spectrum to measure a large separation of 161.1 μHz. They identified twelve oscillation frequencies with l = 0–2, although the high sidelobes from their single-site observations, coupled with the relatively low signal-to-noise (2.5–3.5), means that these may have been affected by daily aliases. Theoretical modelling of α Cen A and B has been carried out several times, most recently by Eggenberger et al. (2004), who also give a thorough review of previous work.

Here we report observations of α Cen B made from two sites that show oscillations clearly and allow us to measure their frequencies, amplitudes and mode lifetimes.

2. VELOCITY OBSERVATIONS AND POWER SPECTRA

We observed α Cen B in May 2003. At the European Southern Observatory in Chile we used UVES (UV-Visual Echelle Spectrograph) at the 8.2-m Unit Telescope 2 of the Very Large Telescope (VLT)[6]. At Siding Spring Observatory in Australia we used UCLES (University College London Echelle Spectrograph) at the 3.9-m Anglo-Australian Telescope (AAT). In both cases, an iodine cell was used to provide a stable wavelength reference (Butler et al. 1996).

At the VLT we obtained 3379 spectra of α Cen B, with typical exposure times of 4 s and a median cadence of one exposure every 32 s. At the AAT we obtained 1642 spectra, with typical exposure times of 10–12 s (but sometimes as long as 30 s in poor weather) and a median cadence of one exposure every 91 s. Note that, unlike for our observations of α Cen A, UCLES was used in standard planet-search mode. For α Cen A we rotated the CCD by 90 degrees to speed up readout time, but found that this introduced drifts and sudden jumps in the velocities that we believe to be related to the movement of the CCD dewar as liquid nitrogen boiled off and was refilled (Butler et al. 2004).

The resulting velocities are shown in Fig. 1, and the effects of bad weather can be seen (we were allocated five nights with the VLT and eight with the AAT). Both sets of velocities show trends during each night that are presumably due to a combination of instrumental drift and stellar convection noise. To remove these trends, we have subtracted a smoothed version of the data one night at a time, producing the detrended time series shown in Fig. 1. This process of high-pass filtering is not strictly necessary, but it does slightly reduce the noise leaking into higher frequencies that would otherwise degrade the oscillation spectrum.

Note that Fourier analysis on unevenly spaced data cannot use the Fast Fourier Transform (FFT) algorithm. We instead employed the method used for many years by various groups, including our own: we calculated the discrete Fourier transform, but with individual data points being weighted according to their quality (e.g. Deeming 1975; Frandsen et al. 1995).

For about one hour at the end of each night, when α Cen B was inaccessible, we observed the star δ Pav (HR 7665; HIP 99240; G8 V). We obtained a total of 179 spectra with the VLT (median cadence 58 s) and 77 with the AAT (median cadence 181 s). The velocities are shown in Fig. 2 and there is a clear periodicity of about 7 min. We did not expect to be able to measure frequencies with such a limited data set, but we do

[1] Department of Physics and Astronomy, University of Aarhus, DK-8000 Aarhus C, Denmark; hans@phys.au.dk, jcd@phys.au.dk
[2] School of Physics A28, University of Sydney, NSW 2006, Australia; bedding@physics.usyd.edu.au, laszlo@physics.usyd.edu.au
[3] Carnegie Institution of Washington, Department of Terrestrial Magnetism, 5241 Broad Branch Road NW, Washington, DC 20015-1305; paul@dtm.ciw.edu, chris@dtm.ciw.edu
[4] Department of Astronomy, University of California, Berkeley, CA 94720; and Department of Physics and Astronomy, San Francisco, CA 94132; gmarcy@astron.berkeley.edu
[5] Anglo-Australian Observatory, P.O. Box 296, Epping, NSW 1710, Australia; cgt@aaoepp.aao.gov.au
[6] Based on observations collected at the European Southern Observatory, Paranal, Chile (ESO Programme 71.D-0618)

see a clear excess in the power spectrum from the oscillations (Fig. 3), whose amplitudes we discuss in Sec. 5.

Our analysis of the velocities for α Cen B follows the method that we developed for α Cen A (Butler et al. 2004). We have used the measurement uncertainties, σ_i, as weights in calculating the power spectrum (according to $w_i = 1/\sigma_i^2$), but modified some of the weights to account for a small fraction of bad data points. In this case, only three data points from UVES and none from UCLES needed to be down-weighted. After these adjustments, we measured the average noise in the amplitude spectrum at high frequencies (above the stellar signal) to be 1.49 cm s^{-1} for UVES (6–8 mHz) and 4.28 cm s^{-1} for UCLES (4.75–5.50 mHz). Note that we used a lower frequency range to measure the noise in the UCLES data because the sampling time of those observations was significantly longer than for UVES (see above).

The power spectrum of the combined series is shown in the top panel of Fig. 4. We refer to this as the noise-optimized power spectrum because the weights have been chosen to minimize the noise. The noise level in amplitude is 1.39 cm s^{-1} (6–8 mHz). As such, these measurements replace our observations of α Cen A (1.9 cm s^{-1}) as the most precise amplitude spectrum obtained on any star apart from the Sun.

The middle panel of Fig. 4 shows a close-up of the noise-optimized power spectrum. There is a clear series of regular peaks with a spacing of about 81 μHz, and we therefore confirm that the large separation is about 162 μHz, in agreement with the value reported by Carrier & Bourban (2003). The inset shows the spectral window, in which we see prominent sidelobes (38% in power) due to gaps in the observing window.

As for α Cen A, we have also generated a power spectrum in which the weights were adjusted on a night-by-night basis in order to to minimize the sidelobes. The result, which we refer to as the sidelobe-optimized power spectrum, is shown in the bottom panel of the figure. The values for these weight multipliers were: 1.0 for all UCLES nights except the last, which had 0.8; and 3.2, 3.2, 2.3 and 2.3 for the four UVES nights. Adjusting the weights in this way increased the noise level to 2.40 cm s^{-1} (6–8 mHz), but allowed us to identify correctly peaks that might otherwise be obscured by sidelobes from their stronger neighbours (now reduced to 13% in power). In addition, the sidelobe minimization has slightly improved the frequency resolution, with the FWHM of the spectral window decreasing by about 20% (from 1.83 μHz to 1.44 μHz). This is because of the increased weight given to the UCLES data, which covers the longer timespan. Note that the dotted lines in Fig. 4 show our final oscillation frequencies, which are discussed in detail in the next section.

3. OSCILLATION FREQUENCIES

We measured the frequencies of the strongest peaks in the power spectrum in the standard way, using iterative sine-wave fitting. We did this for both the noise-optimized and the sidelobe-optimized power spectra, and the resulting frequencies are plotted in echelle format in Fig. 5. The echelle format takes advantage of the fact that mode frequencies for low-degree p-mode oscillations are approximated reasonably well by the asymptotic relation:

$$\nu_{n,l} = \Delta\nu(n + \tfrac{1}{2}l + \epsilon) - l(l+1)D_0. \quad (1)$$

Here n (the radial order) and l (the angular degree) are integers, $\Delta\nu$ (the large separation) reflects the average stellar density, D_0 is sensitive to the sound speed near the core and ϵ is sensitive to the surface layers.

Symbol size in Fig. 5 indicates the signal-to-noise ratio (SNR) of the peaks, and all peaks with SNR ≥ 2.5 are shown. Many of these represent oscillations but some are artefacts due to the non-linear nature of the iterative fitting method and its interaction with noise. The dotted lines represent a fit to the final frequencies that is discussed below; in this figure, they serve to guide the eye and allow us to identify ridges with angular degrees of l = 0, 1, 2 and 3.

We can see from Fig. 5 that many peaks were identified in both versions of the power spectrum and, not surprisingly, many were only above SNR = 2.5 in the noise-optimized version. However, four peaks that were only significant in the sidelobe-optimized version lie close to the oscillation ridges (three with l = 0 and one with l = 1). The detection of these peaks vindicates our decision to examine the sidelobe-optimized power spectrum.

The next step was to select those peaks that we believe are due to oscillations and reject those due to noise. This is the only subjective part of the process, but is required if we are to measure as many frequencies as possible from our data because at this SNR, not all the extracted peaks will be genuine. Our final set of identified modes is shown in Fig. 6 and Table 1 (and also indicated by the dotted lines in Fig. 4). In some cases the iterative sine-wave fitting produced two peaks (in one case, three) that appear to arise from a single oscillation mode, which is to be expected if we have partially resolved the modes (see Sec. 4 for discussion of the mode lifetimes). In these cases, and in cases where the same peak was detected in both versions of the power spectrum, all peaks are shown in Fig. 5 but they are combined into a single unweighted mean in Fig. 6 and Table 1 (the uncertainties given in the table are discussed below in Sec. 4). We have been conservative in not selecting three peaks outside the main region because we cannot be sure of the curvature of the extrapolated ridge lines. These are: 2827.7 μHz (l = 0?), 5894.9 μHz (l = 2?) and 5973.1 μHz (l = 1?).

Inspection of Fig. 4 shows some apparent mismatches between the peaks in the power spectrum and the dotted lines representing the extracted frequencies. For example, there are enhancements in power at 3600, 3700 and 4050 μHz that do not correspond to identified modes. We noted similar structures in our analysis of α Cen A (Bedding et al. 2004) and the explanation is the same: the interaction of the window function with noise peaks and oscillation peaks. We have verified that the same phenomenon occurs in solar data by analysing segments of the publically-available[7] 805-day series of full-disk velocity observations taken by the GOLF instrument (Global Oscillations at Low Frequencies) on the SoHO spacecraft (Ulrich et al. 2000), which have a sampling time of 80 s. We applied the same sampling window as our observations of α Cen B and the results showed low-level structure in the power spectrum similar to those in Fig. 4. This confirms that such a structure is a natural consequence of the spectral window interacting with multi-mode oscillations having finite lifetimes.

In Fig. 6 the open squares show the frequencies reported by Carrier & Bourban (2003). It is clear that, while they found the correct large separation, there is a shift in their frequencies of one cycle per day (11.57 μHz). This reflects the problem associated with single-site observations, especially when the peaks have low signal-to-noise.

[7] http://www.medoc-ias.u-psud.fr/golf/

As with α Cen A, we note a scatter of the peaks about the ridge lines that is much higher than expected from SNR considerations and which we interpret as being due to the finite lifetime of the modes. We therefore fit to the ridges, in order to obtain more accurate estimates for the eigenfrequencies of the star. In the case of α Cen A (Bedding et al. 2004) we fitted to the frequencies in a two-step process by first fitting the three small separations and then fitting a parabola to the individual frequencies. Here, we adopted a simpler approach that gives almost identical results, in which we fitted directly to the frequencies (see Ulrich 1986). The nine fitted parameters specify: the curvatures of the parabolas (one common value), the large separation at some reference frequency for each l (four values) and the absolute positions of the ridges (four values). The equations for this fit are as follows:

$$\nu_{n,0} = \left[3950.57 + 161.45\,(n-23) + 0.101\,(n-23)^2\right]\ \mu\text{Hz} \quad (2)$$

$$\nu_{n,1} = \left[4026.23 + 161.28\,(n-23) + 0.101\,(n-23)^2\right]\ \mu\text{Hz} \quad (3)$$

$$\nu_{n,2} = \left[4101.41 + 161.63\,(n-23) + 0.101\,(n-23)^2\right]\ \mu\text{Hz} \quad (4)$$

$$\nu_{n,3} = \left[4171.13 + 161.76\,(n-23) + 0.101\,(n-23)^2\right]\ \mu\text{Hz}. \quad (5)$$

We show this fit as the dotted curves in Figs. 5 and 6.

Figure 7 shows the small frequency separations (top panel), the D_0 parameter (middle panel) and the large separations ($\Delta\nu$; bottom panel), using the same definitions as Bedding et al. (2004). Thus, $\delta\nu_{02}$ is the separation between adjacent peaks with $l = 0$ and $l = 2$ and $\delta\nu_{13}$ is the separation between $l = 1$ and $l = 3$. The third small separation, $\delta\nu_{01}$, is the amount by which $l = 1$ modes are offset from the midpoint between the $l = 0$ modes on either side:

$$\delta\nu_{01} = \tfrac{1}{2}\left(\nu_{n,0} + \nu_{n+1,0}\right) - \nu_{n,1}. \quad (6)$$

Since one could equally well define $\delta\nu_{01}$ to be the offset of $l = 0$ modes from the midpoint between consecutive $l = 1$ modes,

$$\delta\nu_{01} = \nu_{n,0} - \tfrac{1}{2}\left(\nu_{n-1,1} + \nu_{n,1}\right), \quad (7)$$

we have shown both versions in Fig. 7 (upper panel). Note that D_0, which is sensitive to the stellar core, corresponds to $\frac{1}{6}\delta\nu_{02}$, $\frac{1}{10}\delta\nu_{13}$ and $\frac{1}{2}\delta\nu_{01}$ and is a constant if the asymptotic relation holds exactly. The solid lines in the top and bottom panels show the separations calculated from the fitted equations (in the bottom panel, only $\Delta\nu_0$ is shown; lines for other l values are almost indistinguishable). The upward trend of $\Delta\nu$ with frequency is responsible for the curvature in the echelle diagram.

In Table 2 we give the large and small frequency separations for α Cen B at a frequency of 4.0 mHz. We also give ϵ, which is a dimensionless quantity commonly used to parameterize the absolute position of the frequency spectrum – see equation (1). We are not able to detect any statistically significant variations in the large separation with angular degree (l); the weighted mean value ($\Delta\nu$) has an uncertainty of 0.04%. We also find that the value of D_0 (as defined above) at 4.0 mHz is the same within uncertainties for all three small separations, and our mean value for D_0 has an uncertainty of 3%. We can therefore place α Cen B in the so-called asteroseismic H-R diagram (Christensen-Dalsgaard 1984; see also Ulrich 1986; Gough 2003; Otí Floranes et al. 2005), and these frequency separations should be compared with theoretical models.

Detailed modelling of the α Cen system was carried out by Eggenberger et al. (2004). They determined the parameters of the system through a least-squares fit to the observed quantities, including both 'classical' photometric and spectroscopic data and oscillation frequencies from Bouchy & Carrier (2002) and Carrier & Bourban (2003). Their two preferred models (Models M1 and M2) both have an age of 6.5 Gyr. For α Cen B they obtained large separations $\Delta\nu_0$ of 161.7 and 161.1 μHz, respectively, while the $l = 0$ to 2 small separations were $\delta\nu_{02} = 10.3$ and 10.2 μHz, respectively; both are essentially consistent with the values found here (cf. Table 2), although with some slight preference for Model M1. It should be noted, however, that the average values of these quantities depend on the detailed way in which the averages are computed, including the selection of modes. Also, the computed values of $\Delta\nu_0$, and to a lesser extent $\delta\nu_{02}$, are affected by the uncertain physics of the near-surface layers of the model. An analysis of the combined set of frequencies for α Cen A, presented by Bedding et al. (2004), and the results of α Cen B shown in Table 1 is in progress.

3.1. *Curvature at high and low frequencies*

We now describe a method that allows us to measure the oscillations at low SNR, outside the central region in which we can identify individual modes. This allows us to examine curvature in the echelle diagram, which corresponds to measuring the large separation as a function of frequency. The method relies on smoothing the power spectrum in order to increase the contrast between the oscillation signal and the background noise. The first step was to smooth the power spectrum quite heavily, with a FWHM of $\Delta\nu/4$. This type of smoothing was used by García et al. (1998) to find high-frequency peaks in the solar power spectrum, but here we use an even broader smoothing function. The smoothing combines the power from each even-degree pair of modes ($l = 0$ and 2) into a single resolution element, and the same applies to the odd-degree pairs ($l = 1$ and 3).

We next arranged the smoothed power spectrum in echelle format, with frequencies reduced modulo $\frac{1}{2}\Delta\nu$ rather than the conventional $\Delta\nu$. This causes power associated with odd and even pairs to line up, allowing us to smooth in the vertical direction in this echelle diagram to improve the contrast further (for this smoothing we used FWHM = $3.4\Delta\nu$). Finally, we measured the highest peak in each half-order and these are marked by the open circles in Fig. 8. We see a clear ridge of power that extends well beyond the central region. The dotted lines are the fits shown in Fig. 6 and given by equations (2)–(5). We see good agreement in the central region, but the smoothed data allow us to measure curvature well outside the region in which we were able to identified individual oscillation modes.

In order to evaluate this method, we have also applied it to the oscillations in the Sun by analysing the 805-day GOLF series (see Sec. 3). We used the same amount of smoothing as for α Cen B (when specified in terms of $\Delta\nu$) and the filled circles in Fig. 9 show the highest peak in each half-order. The figure also shows published solar frequencies for $l = 0$–3 (Lazrek et al. 1997; Bertello et al. 2000; Chaplin et al. 2002). We see that the ridge of power follows the published frequencies very well, but again extends beyond them at high frequencies. It is interesting that our measurements at high frequency match up perfectly with the so-called pseudo-modes, also called HIPs (High-frequency Interference Peaks), which have been seen in smoothed solar power spectra up to 7.5 mHz (García et al. 1998; Chaplin et al. 2001; Gelly et al. 2002). This may be relevant to the discussion of the physical nature of these HIPs: are they related to ordinary resonant p modes, despite having frequencies above the acoustic cut-off frequency in the atmosphere, and caused by small but non-zero reflectivity at the photosphere

(Balmforth & Gough 1990); or are they resonances between direct and reflected waves from a localized source (e.g., Kumar et al. 1990; Kumar & Lu 1991)?

The points in Fig. 10 show the large separation as a function of frequency for both α Cen B and the Sun. These values were derived from Figs. 8 and 9, respectively, simply by doubling the differences between consecutive points along the ridges. The two curves are remarkably similar, except for the pronounced dip at 6 mHz in α Cen B, which occurs in the region of low S/N and which we suspect is not real. In fact, our tests show that this type of feature sometimes appears as an artifact when the method is applied to short segments of the solar GOLF data (to match the observing window of α Cen B). The same tests also show that the method does measure $\Delta\nu$ very accurately in the regions where oscillations have significant amplitude. To illustrate this, the dashed lines in Fig. 10 show our best estimates, based on these tests, of the $\pm 1\sigma$ uncertainties in $\Delta\nu$. We conclude that this is a powerful technique for measuring the large separation over an extended frequency range. For α Cen B this will provide extra constraints on theoretical models while, for the Sun, we have been able to measure $\Delta\nu$ to much higher frequencies than has been done previously. The S-shaped structure in the echelle diagram indicates a departure from the second-order fit used in equations (2)–(5), implying that cubic (or higher) terms are needed to describe the frequencies fully. As pointed out by Ulrich (1988), these higher-order coefficients might be useful in constraining the stellar mass.

4. MODE LIFETIMES

The scatter of the observed frequencies about the ridges allows us to estimate the mode lifetimes. In the case of α Cen A we did this by measuring the deviations of the measured frequencies from the fitted relations and comparing with simulations (Bedding et al. 2004). Here we adopted a slightly different approach that has the advantage of being independent of the fit, although it does still assume that we have correctly assigned n and l values. For each measured frequency $\nu_{n,l}$ (solid points in Fig. 6), except those at the ends of the ridges, we calculated the difference $\Delta_{n,l}$ between the measured frequency and that expected from the positions of the two nearest neighbours on the same ridge, using linear interpolation:

$$\Delta_{n,l} = \nu_{n,l} - \frac{\Delta n_- \, \nu_{(n+\Delta n_+),l} + \Delta n_+ \, \nu_{(n-\Delta n_-),l}}{\Delta n_+ + \Delta n_-}. \qquad (8)$$

Here, the two neighbouring modes lie in orders $n+\Delta n_+$ and $n-\Delta n_-$, respectively. In most cases, Δn_- and Δn_+ are 1, but in some cases one or both is 2 or even 3. We therefore need to convert $\Delta_{n,l}$ to a quantity that we can easily compare with simulations. We choose this to be the rms scatter of that peak about its expected position, calculated as follows:

$$\sigma^2_{n,l} = \frac{(\Delta_{n,l})^2 \, (\Delta n_- + \Delta n_+)^2}{(\Delta n_- + \Delta n_+)^2 + (\Delta n_-)^2 + (\Delta n_+)^2}. \qquad (9)$$

Averaging σ over many peaks gives an estimate of the mode lifetime, but we must keep in mind that the finite SNR also introduces a scatter to the peak positions. To calibrate these two contributions, we carried out a large number of simulations (175 000), each with a single input frequency and each sampled with our observational window function (with the noise-optimized weights). We used the method described by Stello et al. (2004) to generate the time series of an oscillation that was re-excited continuously with random kicks and damped on a timescale that was an adjustable parameter (the mode lifetime). The other adjustable input parameter was the oscillation amplitude, while the mode frequency and the noise level were fixed. We made 100 simulations for each set of input parameters and from the resulting power spectra we measured the rms scatter in frequency of the highest peak and its mean SNR (discarding peaks with frequencies more than 4σ from actual value). We repeated this for various values of the input parameters and the results are summarised in Fig. 11. Each solid line in this figure shows the observed frequency scatter versus the observed SNR for a given value of the mode lifetime. As expected, the frequency scatter increases both with decreasing mode lifetime and with decreasing SNR. We stress that this figure applies specifically to our observing window for α Cen B and should be recalculated for other observing windows.

The crosses in Fig. 11 show our results for α Cen B in two frequency ranges, centred at 3.6 mHz (the mean of all peaks below 4.0 mHz) and at 4.6 mHz (the mean of peaks above 4.0 mHz). From these crosses we can determine the mode lifetimes. In order to check our results, we have also analysed segments of the same 805-day GOLF series of full-disk velocity observations of the Sun used in Sec. 3.1. We divided this series into 100 segments, and imposed on each the α Cen B window function (with weights). The squares in Fig. 11 show the frequency scatter for each $l = 1$ mode as a function of the mean SNR (both measured over the 100 segments). We analysed twelve $l = 1$ modes ($n = 16$–27) and ignored the pairs with $l = 0$ and 2 because they are less well resolved and interact via daily sidelobes. We see the well-known result that mode lifetimes in the Sun vary with frequency (the shortest lifetimes occur at the highest frequencies). Those with intermediate frequency have the best SNR because they have the highest amplitudes.

For each measured point in Fig. 11 (two for α Cen B and twelve for the Sun), we used our simulations to infer the mode lifetime. The results are shown as a function of frequency in Fig. 12 using the same symbols, where we have expressed frequency in units of $\nu_{\max}$, the frequency of maximum oscillation power (see Table 3 for values of $\nu_{\max}$). The diamonds in this figure are published measurements of the solar mode lifetimes (Chaplin et al. 1997), and we see good agreement with our values. We also see that the typical mode lifetimes for α Cen B, when considered as a function of $\nu/\nu_{\max}$, are similar to those in the Sun. Our estimates are $3.3^{+1.8}_{-0.9}$ d at 3.6 mHz and $1.9^{+0.7}_{-0.4}$ d at 4.6 mHz.

4.1. *Revised mode lifetimes for α Cen A*

The grey crosses in Fig. 12 show mode lifetimes for α Cen A, based on the observations analysed by Bedding et al. (2004). Here, we have re-measured the mode lifetimes using the method described above, which involved making a whole new series of simulations with the α Cen A window function in order to convert frequency scatters into lifetimes. The inferred lifetimes are $2.3^{+1.0}_{-0.6}$ d at 2.1 mHz and $2.1^{+0.9}_{-0.5}$ d at 2.6 mHz.

We can compare these revised lifetimes for α Cen A with those we reported previously from the same data (see Table 3 in Bedding et al. 2004): $1.4^{+0.5}_{-0.4}$ d at 2.1 mHz and $1.3^{+0.5}_{-0.4}$ d at 2.6 mHz. The revised values are higher, although the 1σ error bars do overlap. The reason for the change is that our previous calculation underestimated the contribution of SNR to the frequency scatter. We did of course include the effects of SNR, but did so by treating it as being independent of the scatter introduced by finite mode lifetimes. In fact, as our new simulations show, the two contributions are not independent. If they were,

the curves in Fig. 11 would not rise towards low SNR as steeply as they do.

The important conclusion, as we can see from Fig. 12, is that mode lifetimes in α Cen A are not substantially lower than those in the Sun, although the value for the lower frequency range is still about 1.5σ below solar.

5. AMPLITUDES AND NOISE LEVELS

It is important to measure oscillation amplitudes in solar-like stars and to compare these with theoretical calculations (e.g., Houdek et al. 1999). It is also interesting to measure the background noise from stellar convection, although in velocity this requires extremely precise measurements because the signature is weak. For both these measurements, we have chosen to smooth the power spectrum heavily, so as to produce a single hump of excess power that is insensitive to the fact that the oscillation spectrum has discrete peaks. It is also useful to convert to power density, which is independent of the observing window and therefore allows us to compare noise levels. This is done by multiplying the power by the effective length of the observing run, which we calculated as the reciprocal of the area under the spectral window (in power).

In Fig. 13 we show smoothed power density spectra for the Sun and four other stars: α Cen A and B, δ Pav and β Hyi. For the four stars, we used the most precise observations available: UVES observations for α Cen B (this paper), δ Pav (this paper) and α Cen A (Butler et al. 2004), and UCLES observations for β Hyi (Bedding et al. 2001). In all cases we used the raw velocity measurements, before removal of any jumps or slow trends, since we are interested in measuring the total noise level.

For the Sun, we used data from BiSON (Birmingham Solar Oscillations Network) and GOLF. The BiSON data comprised a 7-day time series with 40-second sampling from the Las Campanas station in Chile, kindly provided by W. Chaplin (private comm.). The GOLF data comprised a 20-day time series with 20-second sampling, kindly provided by P. Boumier (private comm.). Note that these have a higher Nyquist frequency than the publicly available GOLF data, which we used in Secs. 3.1 and 4 but which are only sampled at 80 s.

The dotted lines in Fig. 13 are fits to the noise backgrounds, based on the Harvey (1984) model of solar granulation. The Harvey model gives a convenient functional form, even in stars where the low-frequency noise has a strong additional contribution from instrumental noise. We discuss the noise levels in more detail below. First, we show that these smoothed power density spectra provide a powerful way to measure oscillation amplitudes in a way that is independent of mode lifetime.

To do this, we first subtracted the background noise (dotted lines in Fig. 13) from each observed power density spectrum. We only included those parts of the spectrum that were at least twice the noise level. In order to calculate the amplitude per oscillation mode, we should then multiply by $\Delta\nu/4$ (where $\Delta\nu$ is the large frequency separation of the star) and take the square root. The rationale for this is that there are four modes in each segment of length $\Delta\nu$ (with l = 0, 1, 2 and 3). However, we must keep in mind that modes with different angular degrees have different visibilities in full-disk observations, due to varying amounts of cancellation. Based on the results presented by Bedding et al. (1996), we calculated the effective number of modes per $\Delta\nu$, normalised to the mean of the l = 0 and l = 1 amplitudes, to be 3.0. We therefore used this factor, rather than 4, in our calculation.

For $\Delta\nu$ we used the following values: 135 μHz for the Sun; 106 μHz for α Cen A; 162 μHz for α Cen B; 56 μHz for β Hyi and 93 μHz for δ Pav. The last of these is not a measurement, since none is available, and is instead derived from the following adopted parameters: $M = 0.9\,M_\odot$, $L = 1.3\,L_\odot$ and $T_{\rm eff} = 5540$ K.

Our amplitude estimates are shown in Fig. 14, and the height, frequency and FWHM of the envelopes are given in Table 3. We see a number of interesting things from Figs. 13 and 14. Looking first at the Sun, the results illustrate very nicely that the solar oscillation amplitude depends on the spectral line that is being measured (see Baudin et al. (2005) for a recent study of this phenomenon). The sodium line used by GOLF is formed higher in the solar atmosphere than the potassium line used by BiSON, which is why GOLF measures higher oscillation amplitudes (Isaak et al. 1989). The actual height difference is difficult to estimate; Palle et al. (1992) quoted $\sim$200 km while Baudin et al. (2005) adopted $\sim$60 km. Velocity measurements of other stars are made using a wide wavelength range so as to include many spectral lines, and the Doppler signal is dominated by neutral iron lines. Since these lines are formed about 400 km below the sodium D lines (Eibe et al. 2001; Meunier & Kosovichev 2003), we would expect solar amplitudes measured using the iodine technique to be less than those from both BiSON and GOLF.

Unfortunately, there do not appear to be any published estimates of the solar oscillation amplitude using the stellar technique. Here we present some previously unpublished observations of the solar spectrum made using iodine referencing. One of us (J.T.W.) made observations of the Moon using the 0.6 m Coude Auxilliary Telescope (CAT) at Lick Observatory, which fed the Hamilton Spectrometer, a high-resolution (R = 60000) echelle (Vogt 1987). The CAT tracked a fixed point of uniform surface brightness (Archimedes crater) for five consecutive nights near full moon, thus measuring the disk-integrated solar spectrum at night (a technique inspired by McMillan et al. 1993). These velocity measurements allowed us to estimate the solar oscillation amplitude, which we include in Fig. 14 and Table 3. The results support the conclusion that Fe I measurements give lower amplitudes than both GOLF and BiSON. They also place the solar amplitude between those of α Cen A and B, as would be expected given their stellar parameters. It would clearly be valuable to obtain more measurements of the Sun, in order to better calibrate the relationship between stellar and solar amplitudes. The method described here allows us to estimate amplitudes independently of mode lifetime and observing window. Comparing the amplitudes of different stars with theoretical models is the subject of a future paper.

We turn now to the noise levels in the various observations, looking first at low frequencies. The rise in power towards low frequencies seen in Fig. 13 is due to a combination of instrumental drift and stellar background noise. Of course, it is very difficult to distinguish between these two, although in the Sun it is established the solar background is dominant. It therefore seems likely that the low-frequency power from α Cen A is also mostly stellar, given the power density is similar to the Sun (see also Kjeldsen et al. 1999). The same may also be true for α Cen B. We can certainly say that at 1 mHz, the granulation noise in both stars is no greater than is observed in the Sun by GOLF and BiSON.

At the highest frequencies the noise levels are dominated by white noise from photon statistics. We can see that the power

density (which indicates noise per unit observing time) is lowest for BiSON and GOLF, followed by α Cen B (UVES) and α Cen A (UVES). In the last two columns of Table 3 we provide an update to Table 1 of Butler et al. (2004), showing the noise per minute of observing at frequencies just above the p-mode envelope ($2\nu_{\rm max}$) and also, where the sampling allows, at very high frequencies (11 mHz). We should note that the power at high frequencies in the Sun (4–6 mHz), particularly in the sodium line used by GOLF, is dominated by solar noise that presumably arises from chromospheric effects, with only a small fraction being due to coherent p-modes.

6. CONCLUSIONS

Our observations of α Cen B from two sites have allowed us to identify 37 oscillation modes with l = 0–3. Fitting to these modes gave the large and small frequency separations as a function of frequency. We also introduced a new method, involving smoothing in the $\frac{1}{2}\Delta\nu$ echelle diagram, that allowed us to trace the ridges of power, and hence measure the large separation, well beyond the central region.

We inferred the mode lifetimes in two frequency ranges by measuring the scatter of the oscillation frequencies about a smooth trend, based on a calibration involving extensive simulations. We found mode lifetimes in α Cen B, when considered as a function of frequency relative to the maximum power, that are consistent with those seen in the Sun. We applied the same analysis to our observations of α Cen A and deduced revised mode lifetimes that are slightly higher than we previously published (Bedding et al. 2004).

A limited set of observations of the star δ Pav showed oscillations centred at 2.3 mHz with peak velocity amplitudes close to solar. Further observations are needed to determine the large separation and individual mode frequencies in this star.

Finally, we also introduced a new method of measuring oscillation amplitudes from heavily-smoothed power density spectra. We estimated the amplitude per mode of α Cen A and B, β Hyi, δ Pav and the Sun, and pointed out that the results may depend on which spectral lines are used for the velocity measurements.

We thank Alan Gabriel and Patrick Boumier from the GOLF team for useful comments and for providing the GOLF data at 20-second sampling. We also thank Bill Chaplin for providing data from BiSON and for useful discussions. This work was supported financially by the Australian Research Council, by the Danish Natural Science Research Council and by the Danish National Research Foundation through its establishment of the Theoretical Astrophysics Center. We further acknowledge support by NSF grant AST-9988087 (RPB), and by SUN Microsystems.

REFERENCES

Balmforth, N. J., & Gough, D. O., 1990, ApJ, 362, 256.
Baudin, F., Samadi, R., Goupil, M.-J., Appourchaux, T., Barban, C., Boumier, P., Chaplin, W. J., & Gouttebroze, P., 2005, A&A, 433, 349.
Bedding, T. R., Butler, R. P., Kjeldsen, H., Baldry, I. K., O'Toole, S. J., Tinney, C. G., Marcy, G. W., Kienzle, F., & Carrier, F., 2001, ApJ, 549, L105.
Bedding, T. R., Kjeldsen, H., Butler, R. P., McCarthy, C., Marcy, G. W., O'Toole, S. J., Tinney, C. G., & Wright, J. T., 2004, ApJ, 614, 380.
Bedding, T. R., Kjeldsen, H., Reetz, J., & Barbuy, B., 1996, MNRAS, 280, 1155.
Bertello, L., Varadi, F., Ulrich, R. K., Henney, C. J., Kosovichev, A. G., & García, 2000, ApJ, 537, L143.
Bouchy, F., & Carrier, F., 2001, A&A, 374, L5.
Bouchy, F., & Carrier, F., 2002, A&A, 390, 205.
Butler, R. P., Bedding, T. R., Kjeldsen, H., McCarthy, C., O'Toole, S. J., Tinney, C. G., Marcy, G. W., & Wright, J. T., 2004, ApJ, 600, L75.
Butler, R. P., Marcy, G. W., Williams, E., McCarthy, C., Dosanjh, P., & Vogt, S. S., 1996, PASP, 108, 500.
Carrier, F., & Bourban, G., 2003, A&A, 406, L23.
Chaplin, W. J., Elsworth, Y., Isaak, G. R., Marchenkov, K. I., Miller, B. A., & New, R., 2001, In *Helio- and Asteroseismology at the Dawn of the Millenium, Proc. SOHO 10/GONG 2000 Workshop*, ESA SP-464, page 191.
Chaplin, W. J., Elsworth, Y., Isaak, G. R., Marchenkov, K. I., Miller, B. A., New, R., Pinter, B., & Appourchaux, T., 2002, MNRAS, 336, 979.
Chaplin, W. J., Elsworth, Y., Isaak, G. R., McLeod, C. P., Miller, B. A., & New, R., 1997, MNRAS, 288, 623.
Christensen-Dalsgaard, J., 1984, In Mangeney, A., & Praderie, F., editors, *Workshop on Space Research in Stellar Activity and Variability*, page 11. Meudon: Observatoire de Paris.
Deeming, T. J., 1975, Ap&SS, 36, 137.
Eggenberger, P., Charbonnel, C., Talon, S., Meynet, G., Maeder, A., Carrier, F., & Bourban, G., 2004, A&A, 417, 235.
Eibe, M. T., Mein, P., Roudier, T., & Faurobert, M., 2001, A&A, 371, 1128.
Frandsen, S., Jones, A., Kjeldsen, H., Viskum, M., Hjorth, J., Andersen, N. H., & Thomsen, B., 1995, A&A, 301, 123.
García, R. A., Pallé, P. L., Turck-Chièze, S., Osaki, Y., Shibahashi, H., Jeffries, S. M., Boumier, P., Gabriel, A. H., Grec, G., Robillot, J. M., Roca Cortés, T., & Ulrich, R. K., 1998, ApJ, 504, L51.
Gelly, B., Lazrek, M., Grec, G., Ayad, A., Schmider, F. X., Renaud, C., Salabert, D., & Fossat, E., 2002, A&A, 394, 285.
Gough, D. O., 2003, Ap&SS, 284, 165.
Harvey, J. W., 1984, In Noyes, R. W., & Rhodes, E. J., editors, *Probing the depths of a star: the study of solar oscillations from space*. JPL 400-237, NASA, JPL, Los Angeles.
Houdek, G., Balmforth, N. J., Christensen-Dalsgaard, J., & Gough, D. O., 1999, A&A, 351, 582.
Isaak, G. R., McLeod, C. P., Pallé, P. L., van der Raay, H. B., & Roca Cortés, T., 1989, A&A, 208, 297.
Kjeldsen, H., Bedding, T. R., Frandsen, S., & Dall, T. H., 1999, MNRAS, 303, 579.
Kumar, P., Duvall, T. L., Harvey, J. W., Jefferies, S. M., Pomerantz, M. A., & Thompson, M. J., 1990, In Osaki, Y., & Shibahashi, H., editors, *Proc. Oji Int. Seminar, Progress of Seismology of the Sun and Stars*, Lecture Notes in Physics, Vol. 367, page 87. Berlin: Springer.
Kumar, P., & Lu, E., 1991, ApJ, 375, L35.
Lazrek, M., Baudin, F., Bertello, L., Boumier, P., Charra, J., Fierry-Fraillon, D., Fossat, E., Gabriel, A. H., García, R. A., Gelly, B., Gouiffes, C., Grec, G., Palle, P. L., Perez Hernandez, F., Regulo, C., Renaud, C., Robillot, J.-M., Roca Cortes, T., Turck-Chieze, S., & Ulrich, R. K., 1997, Sol. Phys., 175, 227.
McMillan, R. S., Moore, T. L., Perry, M. L., & Smith, P. H., 1993, ApJ, 403, 801.
Meunier, N., & Kosovichev, A., 2003, A&A, 412, 541.
Otí Floranes, H., Christensen-Dalsgaard, J., & Thompson, M. J., 2005, MNRAS, 356, 671.
Palle, P. L., Regulo, C., Roca-Cortes, T., Sanchez-Duarte, L., & Schmider, F. X., 1992, A&A, 254, 348.
Stello, D., Kjeldsen, H., Bedding, T. R., De Ridder, J., Aerts, C., Carrier, F., & Frandsen, S., 2004, Sol. Phys., 220, 207.
Ulrich, R. K., 1986, ApJ, 306, L37.
Ulrich, R. K., 1988, In Christensen-Dalsgaard, J., & Frandsen, S., editors, *Proc. IAU Symp. 123, Advances in Helio- and Asteroseismology*, page 299. Dordrecht: Kluwer.
Ulrich, R. K., García, R. A., Robillot, J.-M., Turck-Chièze, S., Bertello, L., Charra, J., Dzitko, H., Gabriel, A. H., & Roca Cortés, T., 2000, A&A, 364, 799.
Vogt, S. S., 1987, PASP, 99, 1214.

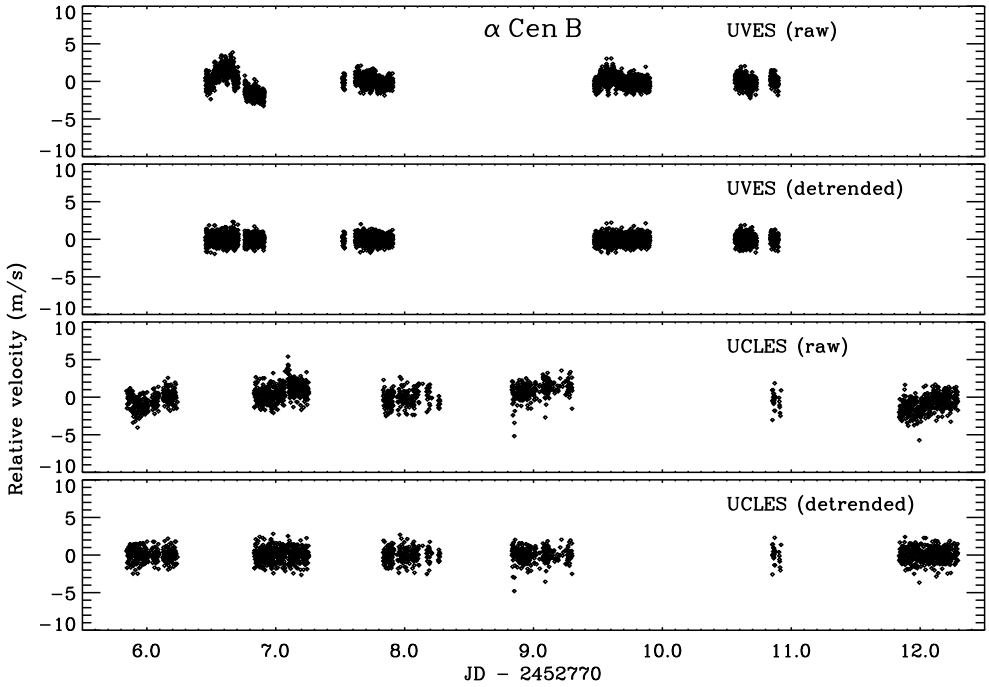

FIG. 1.— Time series of velocity measurements of α Cen B, both before and after removal of slow trends.

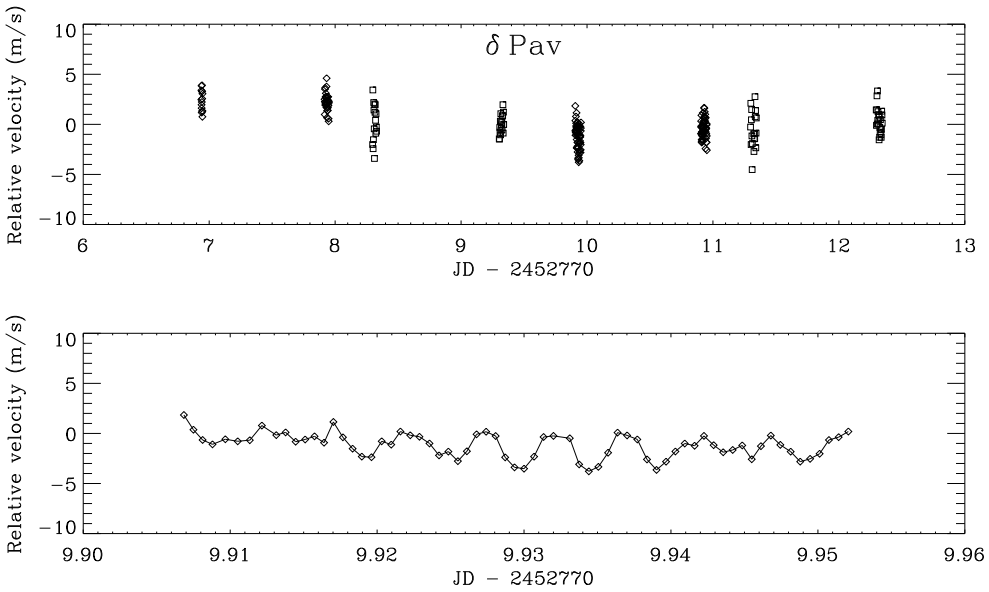

FIG. 2.— Time series of velocity measurements of δ Pav from UVES (diamonds) and UCLES (squares). The lower panel shows a 1.1-hr segment of UVES velocities, in which the 7-min periodicity is clearly visible.

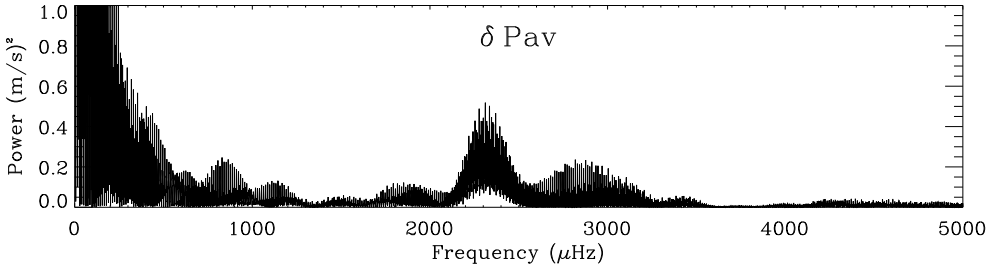

FIG. 3.— Power spectrum of velocity measurements of δ Pav from UVES and UCLES. There is a clear power excess at 2–3 mHz.

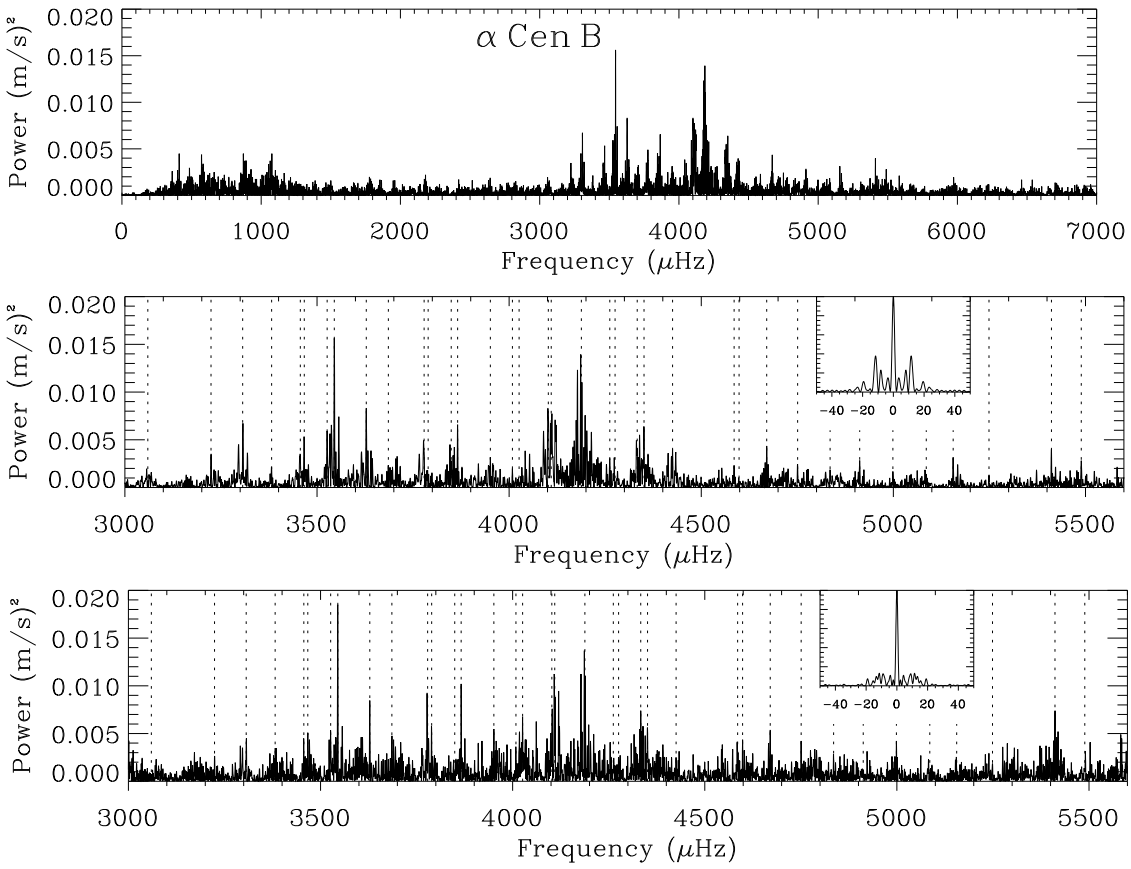

FIG. 4.— Power spectrum of α Cen B from the combined UVES and UCLES data. Top panel: the noise-optimized power spectrum, in which weights were based on the measurement uncertainties, which minimizes the noise. Middle panel: same as top panel, but expanded to show only the central region. Bottom panel: the sidelobe-optimized power spectrum, in which weights were adjusted to minimize the aliases. The spectral windows are shown as insets and vertical dotted lines show our final oscillation frequencies, as listed in Table 1.

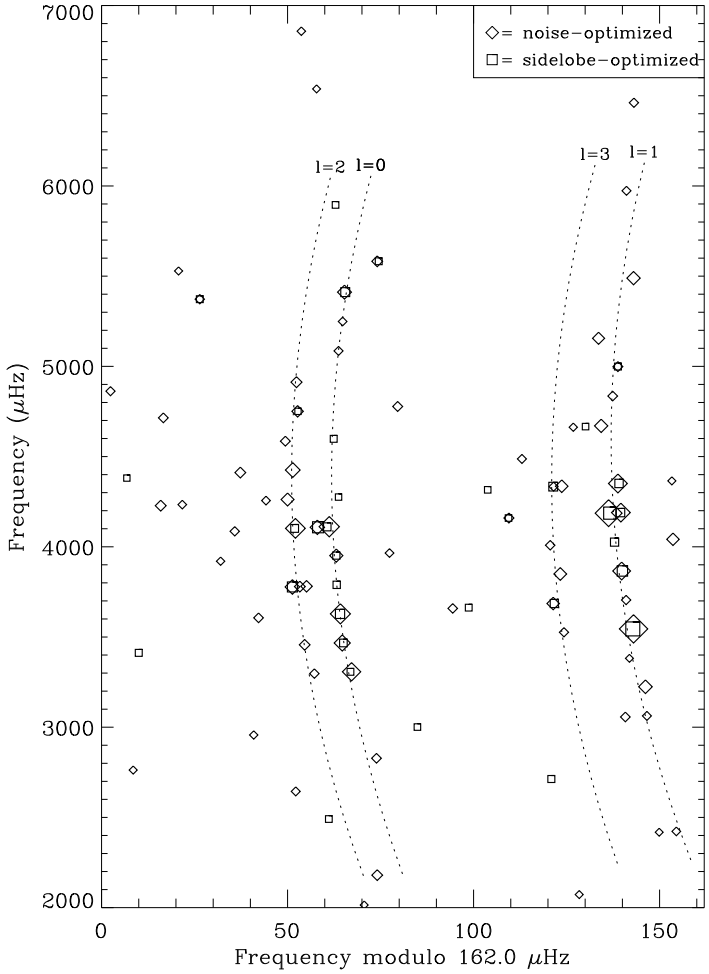

FIG. 5.— Peaks extracted by iterative sine-wave fitting to the α Cen B power spectra, displayed in echelle format. Diamonds and squares, respectively, show peaks extracted from the noise-optimized and sidelobe-optimized power spectra. Symbol sizes are proportional to the SNR of the peaks. The dotted curves are fits to the final frequencies, given by equations (2)–(5).

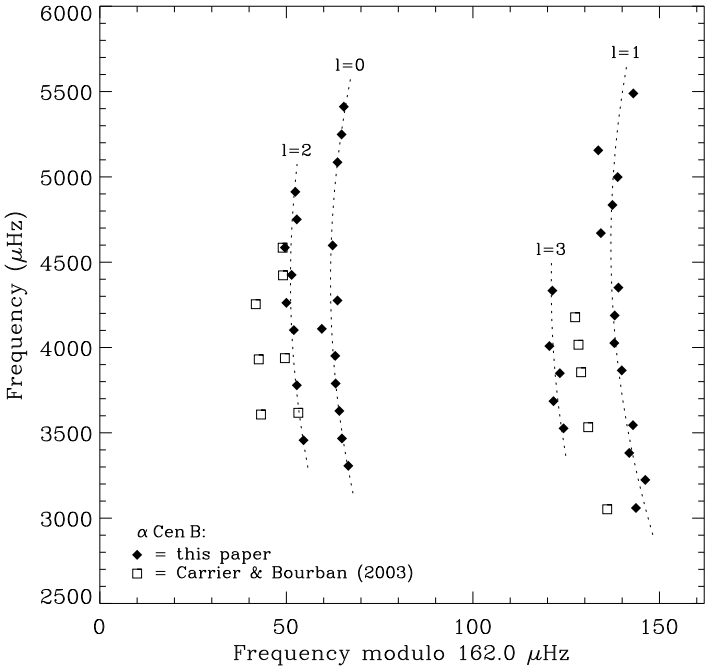

FIG. 6.— Echelle diagram of the final oscillation frequencies in α Cen B (filled diamonds), as listed in Table 1. Dotted curves show the fits to the frequencies, given by equations (2)–(5). Open squares indicate the frequencies reported by Carrier & Bourban (2003).

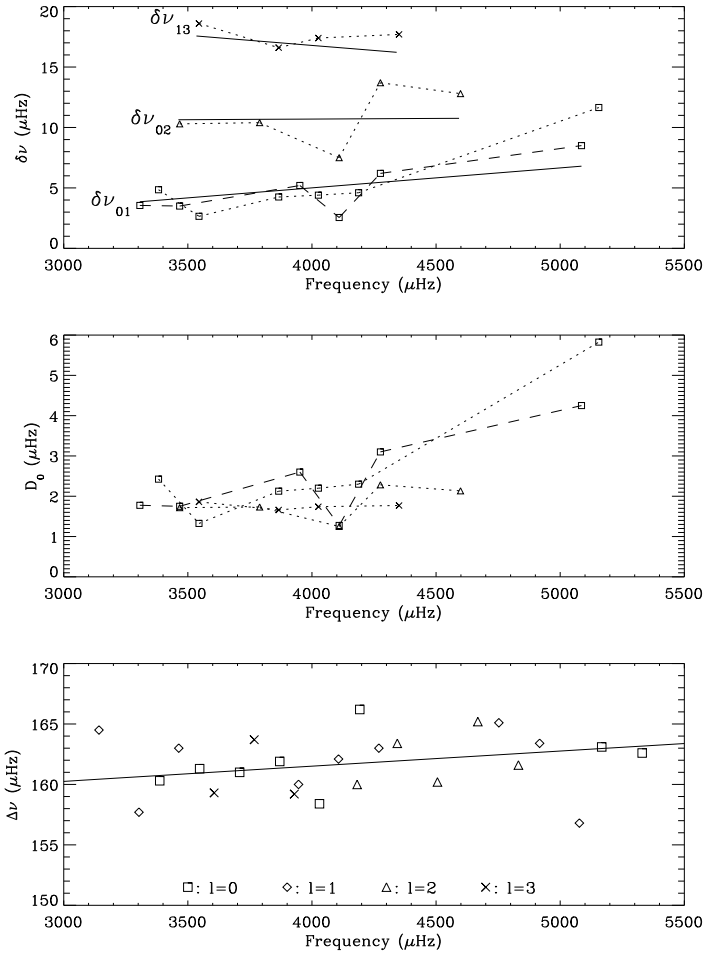

FIG. 7.— Frequency separations for α Cen B. Top panel: small frequency separations, including $\delta\nu_{01}$ from both equations (6) and (7) (the dashed line connects the latter values). Solid lines show the separations calculated from equations (2)–(5). Middle panel: the D_0 parameter, calculated as $\frac{1}{6}\delta\nu_{02}$, $\frac{1}{10}\delta\nu_{13}$ and $\frac{1}{2}\delta\nu_{01}$, with symbols (and line styles) showing the corresponding separations in the top panel. Bottom panel: the large separations for each value of l, with the solid line showing $\Delta\nu_0$ as calculated from equation (2).

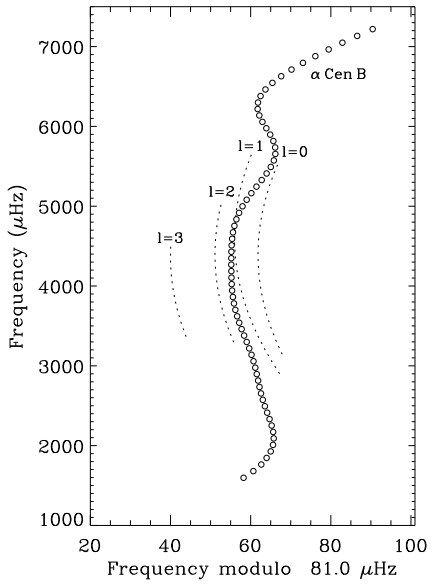

FIG. 8.— Smoothed echelle diagram of the power spectrum of α Cen B, plotted with frequencies reduced modulo half the large separation (see Sec. 3.1 for details). The dotted lines correspond to the fits shown in Fig. 6 and given by equations (2)–(5).

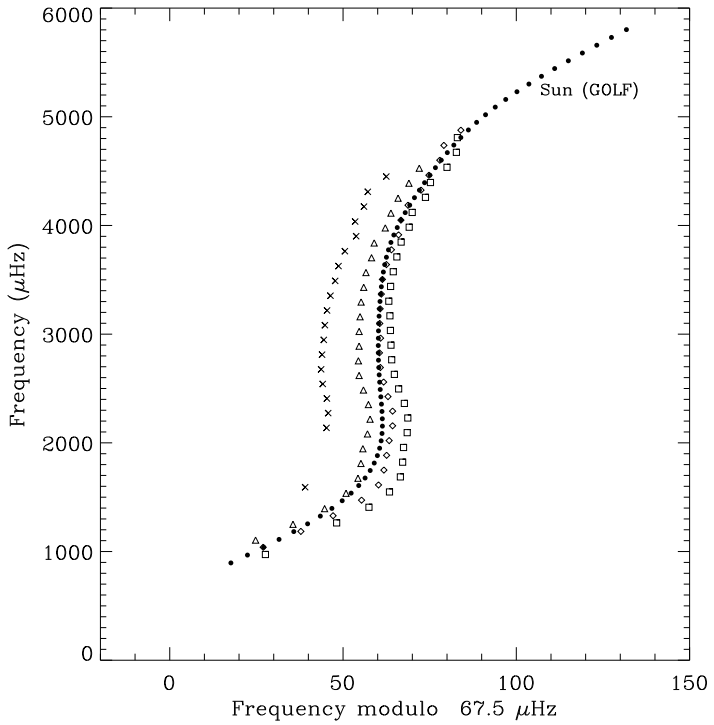

FIG. 9.— Similar to Fig. 8, but for a 805-day series of GOLF observations of the Sun. The open symbols are published solar frequencies for different l values (open symbols have same meaning as in the bottom panel of Fig. 7).

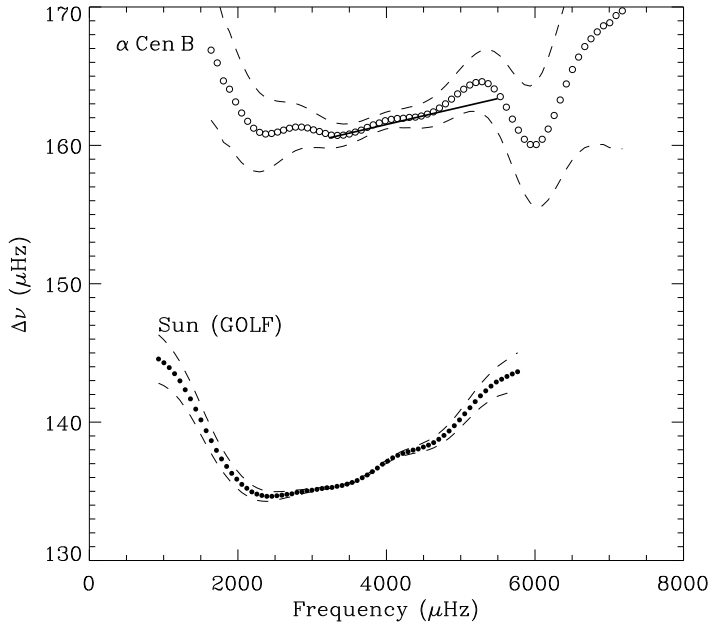

FIG. 10.— The large separation as a function of frequency in α Cen B and the Sun, as derived from Figs. 8 and 9. The dashed lines indicate the $\pm 1\sigma$ uncertainties on $\Delta\nu$ (see text). The solid line for α Cen B is the same as in the bottom panel of Fig. 7 and shows $\Delta\nu_0$ as calculated from equation (2).

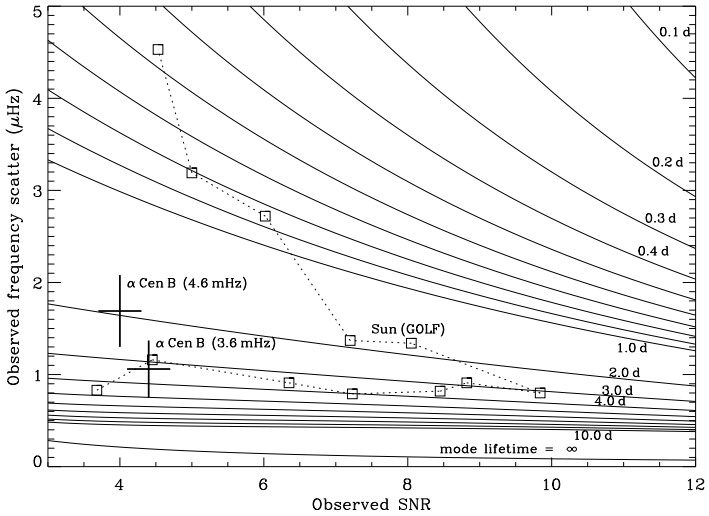

FIG. 11.— Calibration of mode lifetimes for the α Cen B observing window, using the noise-optimized weights. Solid lines are the results of simulations and show frequency scatter versus SNR for various mode lifetimes. Crosses show actual results for α Cen B in two frequency ranges, while open squares show results from GOLF data for twelve consecutive $l = 1$ modes in the Sun.

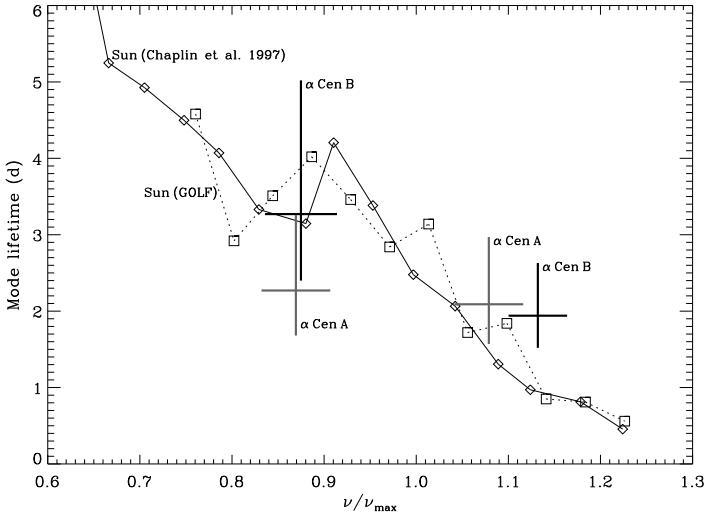

FIG. 12.— Mode lifetimes versus normalized frequency, where $\nu_{\max}$ is the frequency of maximum oscillation power. Values for α Cen B (black crosses) and the Sun observed by GOLF (open squares) are calculated from Fig. 11. Two values for α Cen A (grey crosses) are calculated from a similar calibration of the results presented by Bedding et al. (2004). Open diamonds are published measurements of the solar mode lifetimes (Chaplin et al. 1997).

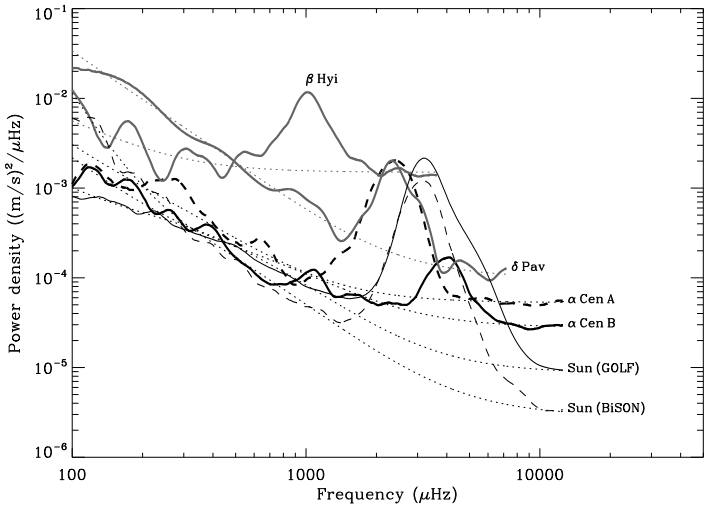

FIG. 13.— Smoothed power density spectra from velocity observations of the Sun and four other stars. The dotted lines are fits to the noise background.

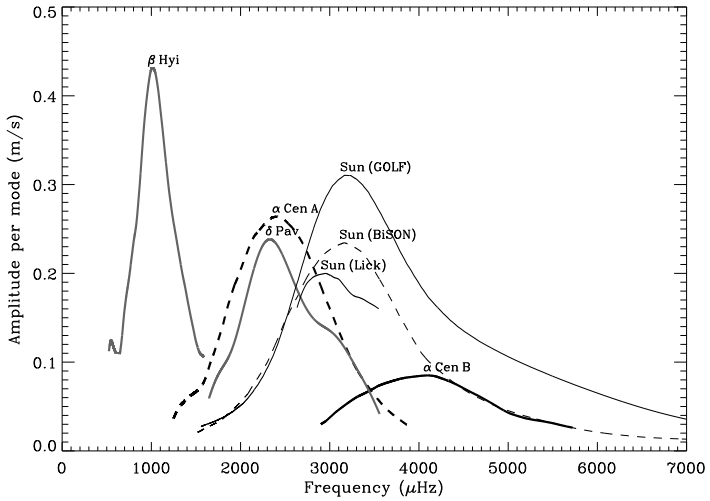

FIG. 14.— Amplitude per mode for solar-like oscillations. These curves were calculated from those in Fig. 13 by subtracting the background noise, multiplying by $\Delta\nu/3.0$ and taking the square root (see text). We also show oscillation amplitudes in the Sun, measured from iodine-referenced observations at Lick Observatory.

TABLE 1
OSCILLATION FREQUENCIES FOR α CEN B (μHZ)

n	$l = 0$	$l = 1$	$l = 2$	$l = 3$
17	...	3059.7 ± 0.9	...	...
18	...	3224.2 ± 0.9	...	...
19	3306.6 ± 0.9	3381.9 ± 1.1	3456.6 ± 1.1	3526.3 ± 1.1
20	3466.9 ± 1.0	3544.9 ± 0.8	...	3685.6 ± 1.1
21	3628.2 ± 1.0	...	3778.8 ± 1.1	3849.3 ± 1.3
22	3789.2 ± 1.2	3865.9 ± 1.1	...	4008.5 ± 1.5
23	3951.1 ± 1.2	4025.9 ± 1.2	4102.0 ± 1.2	...
24	4109.5 ± 1.1	4188.0 ± 1.1	4262.0 ± 1.5	4333.3 ± 1.4
25	4275.7 ± 1.5	4351.0 ± 1.4	4425.4 ± 1.5	...
26	...	...	4585.6 ± 1.8	...
27	4598.4 ± 1.6	4670.3 ± 1.7	4750.8 ± 1.8	...
28	...	4835.4 ± 2.0	4912.4 ± 2.0	...
29	...	4998.8 ± 1.9	...	...
30	5085.7 ± 2.2	5155.6 ± 2.1	...	...
31	5248.8 ± 2.4	...	...	...
32	5411.4 ± 1.9	5489.0 ± 2.3	...	...

TABLE 2
FREQUENCY SEPARATIONS AT 4.0 MHZ FOR α CEN B (μHZ)

$\Delta\nu_0$	161.50 ± 0.11	(0.07%)
$\Delta\nu_1$	161.27 ± 0.09	(0.06%)
$\Delta\nu_2$	161.48 ± 0.17	(0.11%)
$\Delta\nu_3$	161.53 ± 0.33	(0.20%)
$\Delta\nu$	161.38 ± 0.06	(0.04%)
$\delta\nu_{01}$	4.52 ± 0.51	(11%)
$\delta\nu_{02}$	10.14 ± 0.62	(6%)
$\delta\nu_{13}$	16.73 ± 0.65	(4%)
D_0	1.771 ± 0.047	(3%)
ϵ	1.477 ± 0.011	(0.7%)

TABLE 3
AMPLITUDES AND NOISE LEVELS FOR SOLAR-LIKE OSCILLATIONS

Star	Spectrograph	Peak amplitude per mode ($m\,s^{-1}$)	ν_{max} (mHz)	FWHM (mHz)	Noise per min ($m\,s^{-1}$) at $2\,\nu_{max}$	at 11 mHz
α Cen B	UVES	0.085 ± 0.004	4.09 ± 0.17	1.98 ± 0.14	0.35	0.32
α Cen A	UVES	0.263 ± 0.008	2.41 ± 0.13	1.34 ± 0.04	0.49	0.45
β Hyi	UCLES	0.432 ± 0.016	1.02 ± 0.05	0.54 ± 0.05	2.47	—
δ Pav	UVES	0.236 ± 0.008	2.33 ± 0.09	1.24 ± 0.06	0.82	—
Sun	GOLF	0.308 ± 0.005	3.21 ± 0.11	1.76 ± 0.02	0.52	0.20
Sun	BiSON	0.233 ± 0.006	3.17 ± 0.13	1.62 ± 0.04	0.20	0.12
Sun	Lick	0.208 ± 0.029	2.95 ± 0.31	—	—	—